Biomechanical analysis of inosculations (self-growing connections) in Ficus benjamina L. Impact of developmental growth levels on mechanical properties

Wang, Xiuli; Gard, Wolfgang; van de Kuilen, Jan Willem

DOI
10.1016/j.conbuildmat.2024.139672

Publication date
2025

Document Version
Final published version

Published in
Construction and Building Materials

Construction and Building Materials 462 (2025) 139672

Contents lists available at ScienceDirect

Construction and Building Materials

journal homepage: www.elsevier.com/locate/conbuildmat

Biomechanical analysis of inosculations (self-growing connections) in *Ficus benjamina* L.: Impact of developmental growth levels on mechanical properties

Xiuli Wang [a,b,*], Wolfgang Gard [a], Jan-Willem van de Kuilen [a,c]

[a] Biobased Structures and Materials, Faculty of Civil Engineering and Geosciences, Delft University of Technology, Delft, The Netherlands
[b] Institute of Bio- and Geosciences, IBG-2: Plant Sciences, Forschungszentrum Jülich GmbH, Jülich, Germany
[c] Wood Technology, Department of Materials Engineering, Technical University of Munich, Munich, Germany

ARTICLE INFO

Keywords:
Adaptive growth
Building with nature
Inosculation
Self-growing connection
Tensile strength

ABSTRACT

Trees can adapt to external loads and form inosculations (self-growing connections), where stems or branches naturally fuse together. However, a limited understanding of biomechanical features of connections hinders their practical applications. This study used connections formed by *Ficus benjamina* L. to investigate their mechanical properties at different growth levels. Two parameters (fusion degree and interface curvature) were identified to describe growth levels. Customized tensile tests were designed to measure mechanical properties perpendicular to the interconnected surface. Growth levels of studied connections ranged from initial formation to almost fusion of piths, which provided a range of tensile strength of 0.23 to 1.38 MPa. Two primary failure modes (failure at the interface and failure across the stems) were found to be linked to growth levels. The fusion degree, at approximately 15%, contributed to distinguishing failure modes. The average diameter of a connection had the most significant effect on its tensile strength and stiffness. Moreover, the interface curvature correlated negatively with mechanical properties. Average diameter, interface curvature, and fusion degree were effective predictors of connections' tensile strength. Regarding *Ficus* connections, dry connections were stronger than wet connections. These findings provide evidence for nature-based design using self-growing connections under different moisture conditions and growth levels.

1. Introduction

The adaptability of trees allows them to optimize their morphology in response to environmental loads (e.g., wind, ice, or snow loading, as well as movements of animals) [1–5]. For instance, under wind loads, plants typically respond to these stimuli by shortening stem elongation and increasing radial growth. This adaptation reduces the slenderness ratio of the stem in order to enhance stability [4,5]. Based on this adaptive growth, trees can incline their stems and fuse with neighboring trees for mutual supports, which results in the formation of inosculations (self-growing connections) between trees [6–9]. During this growing process, trees undergo various changes, from cellular alterations to adjustments in stem geometry [3,4,10,11]. Previous research [6,9,10] has focused on the characterization of the growth characteristics of self-growing connections fused by *Ficus benjamina* L. (Fig. 1a). However, the mechanical properties of these connections are not well understood, which raises doubts about their potential applications.

The interface of a connection is important for its structural and hydraulic connectivity, as well as the developmental growth. Based on previous findings [9,10], when two stems fuse, the contact area creates a 3D saddle-shaped interface (Fig. 1b). In contrast to the linear and regular elements of traditional structures, this irregular shape poses challenges in understanding its growth characteristics and mechanical properties. In a natural environment, as studied in [12] and presented in the image ([6, Fig. 9]), when the intersecting stems of two trees are considered as a structural system, the forces transmitted through the canopy and stem from wind, rain or snow will occur in the nodal region as bending moments, torques, and shear forces simultaneously. This results in a complex stress environment at the interface in combination of shear, tensile, and compressive stresses. To investigate the interface, it is important to understand the material's composition, morphology and geometry in this area.

Regarding the material composition in this intersected area, tension wood is identified, which is accompanied by an expanded volume and

* Corresponding author at: Biobased Structures and Materials, Faculty of Civil Engineering and Geosciences, Delft University of Technology, Delft, The Netherlands.
E-mail addresses: xiu.wang@fz-juelich.de (X. Wang), W.F.Gard@tudelft.nl (W. Gard), vandekuilen@hfm.tum.de (J.-W. van de Kuilen).

https://doi.org/10.1016/j.conbuildmat.2024.139672
Received 29 July 2024; Received in revised form 14 October 2024; Accepted 18 December 2024
Available online 18 January 2025

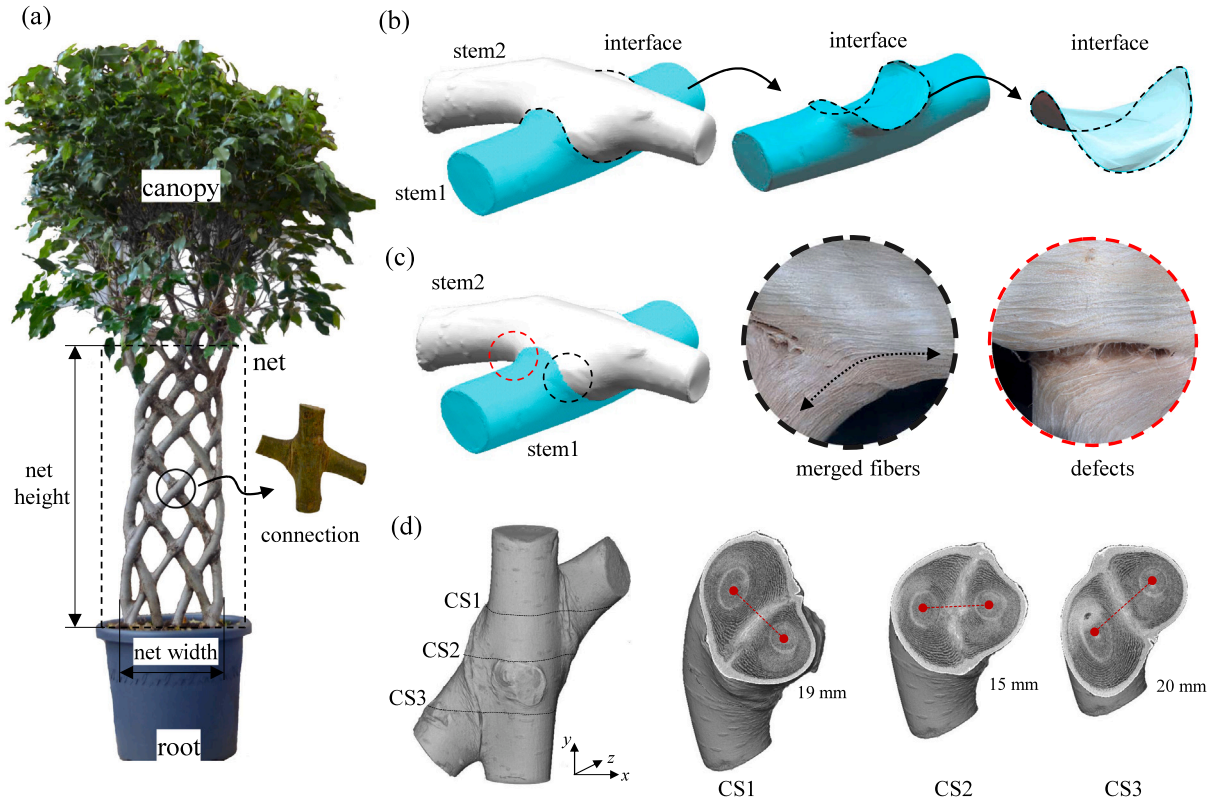

Fig. 1. Structural and growth features of self-growing connections in *Ficus benjamina* L. according to previous studies [9,10]. (a) Overview of *Ficus* trees with a planar pattern; (b) Illustration of the 3D saddle-shaped interface formed between two stems (stem1 and stem2); (c) Detailed view of the merged fibers (left, black circle) and defects (right, red circle) at the interface of the self-growing connection; (d) Cross-sections (CS1, CS2, CS3) of a self-growing connection, indicating the distance between piths and variations in diameter across different sections. (For interpretation of the references to color in this figure legend, the reader is referred to the web version of this article.)

optimized distribution of biomass [10]. This optimization allows for a smooth transition in the intersected area and thus reduces stress concentrations. Meanwhile, it simultaneously connects the growth of two stems (Fig. 1c) [9]. However, according to previous research [9,10], the fiber structure within the interconnected region is not constantly continuous. Continuous fiber tissues are found mainly in the larger transition regions, which guarantees structural and hydraulic integrity (Fig. 1c, area in a black circle). In contrast, in the smaller transition (Fig. 1c, area in a red circle), few continuous fiber tissues are observed, which makes this area vulnerable to splitting. Thus, material defects are considered in this corner in terms of mechanical integrity. In this circumstance, for a natural wood connection, its tensile and shear capacity perpendicular to the intersected surface is crucial to determining its mechanical limits. In other words, the interface is considered weakest in the transverse loading direction due to deviated fiber structures and defects at corners.

However, measuring the mechanical properties of self-growing connections is challenging because of their complex geometry and fiber morphology, as well as different growth levels. Currently, to the best of the authors' knowledge, there is no standardized loading method to comprehensively assess these properties [13,14]. At the material level, testing small wood samples (less than 20 mm in dimension) above fiber-saturated moisture is difficult to prepare proper coupons and ensure accurate measurements. At the connection level, transverse loading tests (i.e., tensile out-of-interface) on irregular connections present numerous challenges. The centerlines of the stems are not aligned in a plane because two single stems have a certain diameter before the formation of a connection. Consequently, this tends to cause an eccentricity when the connection is loaded. Moreover, variations in cross-angle and diameter require flexible clamps. Furthermore, the loading scheme requires forces to transfer effectively to the interface. Therefore, a loading setup that can be adapted to the varying size of connections needs to be designed. Regarding the measuring method, the three-dimensional digital image correlation (3D DIC) is suitable for measuring deformations and strains on irregular surfaces, such as trees [15,16]. Apart from that, considering the impact of the moisture content is crucial, as saturated wood strength is usually considered lower than dry wood. This is related to the mechanical potential of connections in different moisture environments.

The key to understanding the biomechanical performance of a connection lies in linking growth levels to mechanical properties. Regarding developmental growth levels, it is found that the volume, morphology, and composition of the merged fibers play the vital role (Fig. 1c) [9]. These aspects interact with each other during the formation of merged fibers. Furthermore, the amount and orientation of these merged fibers are difficult to quantify in a nondestructive manner. Previous research [10] suggests that the distance between piths (marked in red in Fig. 1d) is correlated with growth levels. The middle location of a connection (CS2) is argued to indicate the position where the fibers are optimally merged between the stems. Therefore, the correlation between geometric dimensions and fiber structures can provide a way to quantify the characteristics of the connected fibers.

Thus, to measure, analyze, and predict the biomechanical performance of self-growing connections, the research objectives of this paper are organized into several steps:

- Identify parameters to quantify the developmental growth levels of a connection following previous research [10].
- Design mechanical tests to measure the strength, stiffness and load-carrying capacity of connections.
- Analyze the difference in failure mechanisms for different levels of growth.

Table 1
General braided information and testing details of braided tree structures.

General information	ID	Full height (mm)	Net size (mm)	Number of tests
Small braided trees	Tree SA	1200–1300	Net width: 200–250; Net height: 600–650; Interval length: 50–150.	4
	Tree SB			4
	Tree SC			6
	Tree SD			6
Big braided trees	Tree BA	1800–2000	Net width: 300–350; Net height: 800–850; Interval length: 100–200.	14
	Tree BB			16
	Tree BC			18
	Tree BD			18
	Tree BE			18
Dry braided trees	Tree DA			9
Total	10	–	–	113

- Establish a predictive relationship between growth-related parameters and mechanical strength.

The adaptive growth and optimization of trees allow them to maintain structural integrity while achieving efficient water transport. This offers valuable insights for bioinspired design in engineering.

2. Materials and methods

2.1. Self-growing connections in different conditions

This research investigated the biomechanics of self-growing connections formed by *Ficus* in a planar braided pattern (Fig. 1a) following previous research [10]. A total of 10 braided tree structures of varying net sizes were utilized. They provided connections at different levels of growth. Table 1 provides details on the braided information of the trees studied. The net size was measured as shown in Fig. 1a. The small braided trees had smaller mean stem diameters of approximately 16 mm, while the big braided trees had mean diameters greater than 20 mm. Each braided tree structure consisted of six stems braided in pairs, creating self-growing connections at intervals of 50 to 200 mm. The connections were studied under two moisture conditions: dry and wet. Wet or green connections were tested immediately after they were cut from the trees. Dry connections were taken from dead trees and kept in a climate-controlled room (21 °C, 65% relative humidity) until the moisture content reached 12%. Green connections were stored in a refrigerator at 0 to 7 °C and covered with a moist cloth soaked in 50% ethanol solution to preserve the moisture content.

The spatial location of a connection may influence its growth condition due to variations in the distribution of biomass and wood properties along the height of the stems. Therefore, the schematic illustration of Tree BA (Table 1) was represented the method to describe its spatial morphology (Fig. 2). As shown in Fig. 2a and b, stems were labeled sequentially from left to right; and connections were labeled from left to right and bottom to top to distinguish the spatial location of each connection. Thus, connections were classified into three regions: lower (1–7), middle (8–14), and upper (15–21). This aims to determine whether the strength varies significantly between these growing regions. The diameter fluctuations and coefficient of variation (CoV) in each stem were further analyzed, as presented in Fig. 2c and d. The analysis confirmed previous results that the production of connections influenced diameter variations more significantly than the tapered shape of the stem [10].

2.2. Measurements of influencing parameters on mechanical properties

To accurately quantify the factors that influence the mechanical properties of the *Ficus* connections, several parameters were measured. These included basic density, moisture content, diameters, diameter ratio, cone ratio, interface area, and cross-angle of a connection. Most importantly, the parameters specific to the growth levels were also evaluated, which included the fusion degree and interface curvature.

Basic density (ρ): The basic density in this study was calculated as the ratio of the dry mass (wood mass) to the green volume, as shown in Eq. (1). Given the irregular shape of the connections, the water displacement method was used to measure the volume. A freshly cut connection was inserted into a beaker filled with water. The volume of water displaced by the connection was considered its green volume. The green mass was determined immediately after cutting the connection from the tree. Following mechanical tests, connections were dried in an oven until a constant dry wood mass was achieved, in accordance with EN13183 standard [17].

$$\rho = \frac{M_d}{V_g}, \tag{1}$$

where ρ represents the basic density of a connection, in kg/m^3; M_d and V_g denote the dry mass and green volume, respectively.

Moisture content (MC): The moisture content was measured by dividing the mass of water in the connection by the dry wood mass, expressed as a percentage in Eq. (2).

$$\mathrm{MC} = \frac{M_g - M_d}{M_d} \times 100\%, \tag{2}$$

where M_g denotes the green wood mass.

Cross-angle (α): This angle was measured between the center lines of the stems, as shown in Fig. 3a. The smaller angle was referred to as the cross-angle of a connection. The cross-angle for the samples ranged from 25 to 90° due to the angle limits of the clamps in the mechanical setup.

Diameter (D), **cone ratio** (R_{cone}), **diameter ratio** (R_{dia}): Diameters of each stem were measured on four sides of a connection: D_{11}, D_{12}, D_{21}, and D_{22}. These measurements were taken 2 to 3 cm from the interface to avoid the enlarged volume near the intersected region [10]. The cone ratio for each stem was calculated by dividing the smaller diameter by the larger diameter. The smaller ratio within two stems was consistently used in subsequent analyses, because the variation in cone ratios across the tested connections was less than 5%. The diameters measured on the two sides in a stem were averaged to determine its diameter. Similarly, the diameter (D_{avg}) of a connection was the mean of stem1 (D_1) and stem2 (D_2). Therefore, the diameter ratio was obtained from the division of the maximum stem size (stem1) divided by the minimum stem size (stem2).

2.3. Parameters describing developmental growth levels

As shown in Fig. 3b, the distance measured at the center and between the edges of two stems in the *xy* plane was referred to as the fusion depth (F). The difference between the sum of the diameters of two stems and the fusion depth was then referred to as the net fusion depth.

Fusion degree (F_d): It was defined as the percentage of the net fusion depth relative to the mean diameter in the connection, as expressed in Eq. (3). The calculation was based on the assumption that combined growth occurs at the interface, as discussed in Fig. 1d and [10]. As a result, the size difference between the interface and diameters of stems

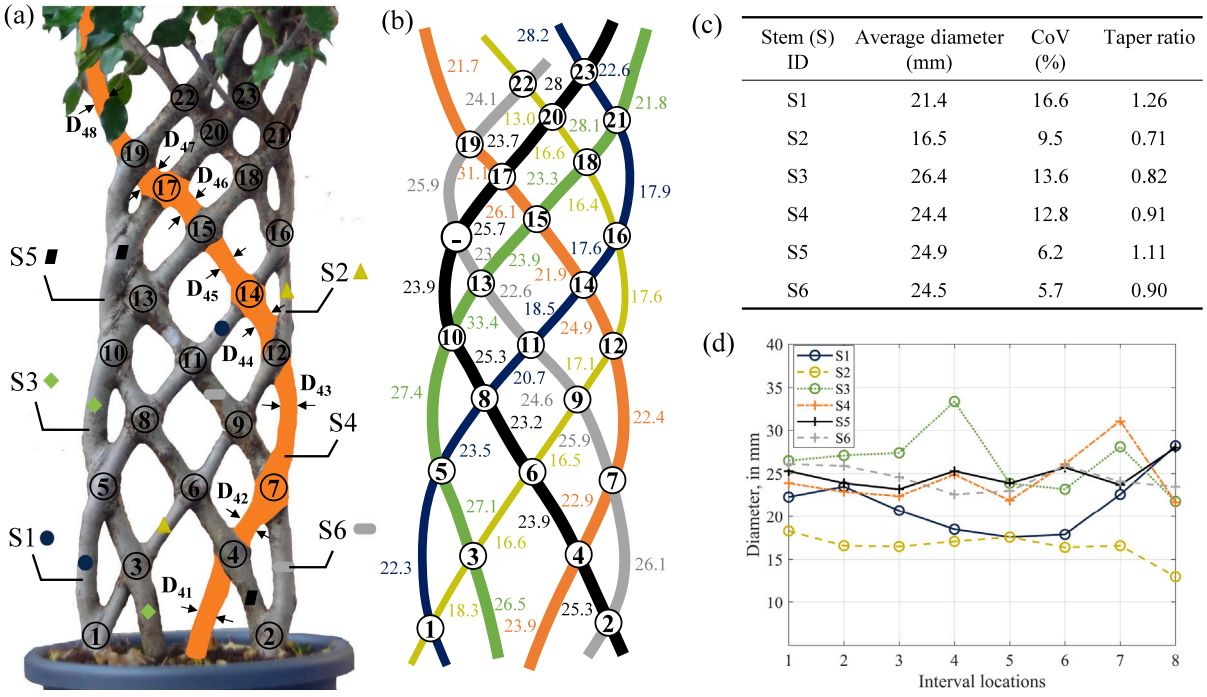

Stem (S) ID	Average diameter (mm)	CoV (%)	Taper ratio
S1	21.4	16.6	1.26
S2	16.5	9.5	0.71
S3	26.4	13.6	0.82
S4	24.4	12.8	0.91
S5	24.9	6.2	1.11
S6	24.5	5.7	0.90

Fig. 2. Spatial morphology and diameter analysis of Tree BA. (a) Schematic illustration of Tree BA with spatial locations of stems and connections. Stems are labeled sequentially from left to right (S1 to S6), and connections are labeled from bottom to top (1 to 23); (b) Detailed diagram of the braided structure with the location of the connection and the respective diameters of the stem at those points; (c) Average diameter, coefficient of variation (CoV), and taper ratio of each stem; (d) Graph showing the diameter fluctuation of each stem across different interval locations.

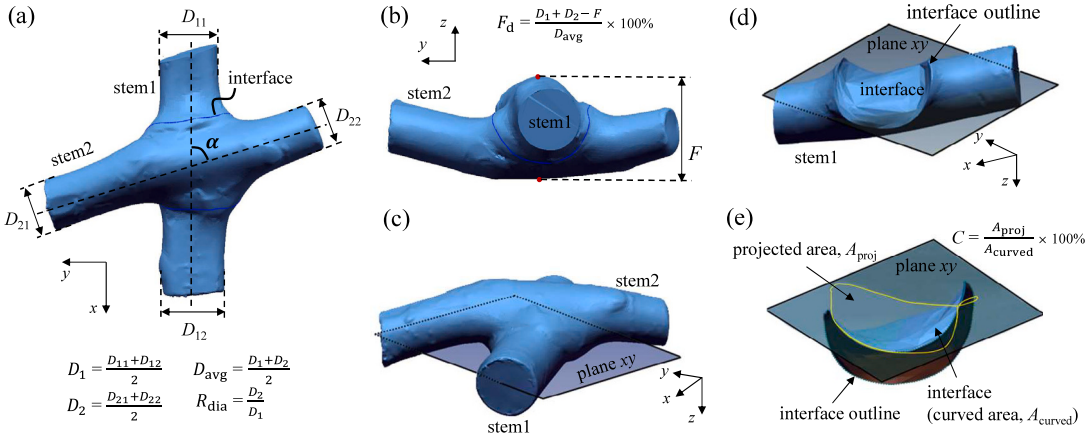

Fig. 3. Measurements on the geometric parameters of a self-growing connection. (a) Measured parameters of a connection, including diameters of four stem parts (D_{11}, D_{12}, D_{21}, D_{22}), cross-angle (α), and the calculation of average diameter (D_{avg}) and diameter ratio (R_{dia}); (b) Measurement method for the fusion degree (F_d); (c) Construction of the loading plane for a connection; (d) Projection relationship between the interface area (A_{curved}) and the loading plane (plane xy); (e) Projected area (effective area, A_{proj}) onto the interface to calculate the strength and the interface curvature (C) of a connection.

indicated the extent of combined growth. In other words, the fusion degree described the extent to which one stem grows together the other, representing the connection's growth level.

$$F_d = \frac{D_1 + D_2 - F}{D_{avg}} \times 100\%, \quad (3)$$

where F_d denotes the fusion degree of a connection, in %; D_1, D_2, and D_{avg} mean the diameters of stem1, stem2 and the mean of two stems' diameters; and F is the measured depth of fusion.

To measure the interface, scanner equipment (HandyScan 3D, Creaform) was utilized to measure the curved area (A_{curved}), with a resolution of 1 mm. The outer layer of a connection was obtained from scanning, as shown in Fig. 3c, and subsequently the data were processed using VXElement to create a mesh model from the point-cloud data. The edge of the connected area (Fig. 3d) was manually identified as a cutting curve to separate two stems and expose to the interface. The 3D surface was reconstructed by selecting the nearest three points to generate a mesh with a resolution of no less than 5 mm^2. Consequently, the curved area was formed and measured (Fig. 3e).

Projected area (A_{proj}): The mapped plane xy was the mechanical loading plane constructed by the center line of one stem with a normal vector perpendicular to the other center line of another stem. The curved interface was then projected to this plane, and the resulting planar surface was measured as the projected area.

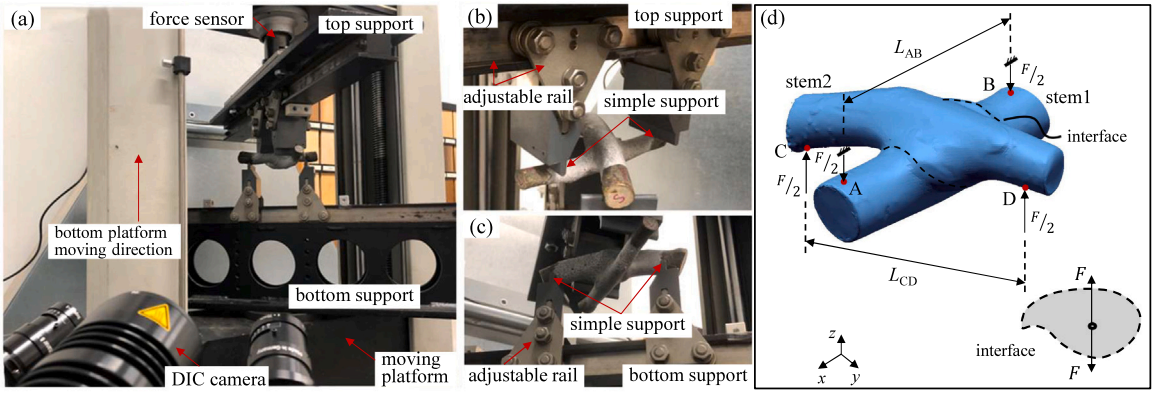

Fig. 4. Experimental setup for tensile out-of-interface tests. (a) Overview of the tensile setup with two rotatable clamps, a force sensor, and DIC for measurements; (b) Details of the top clamp which is not movable in the vertical direction; (c) Details of the bottom clamp which applies forces to the connection by moving in the z direction; (d) Schematic representation of the tensile load transfer on the connection. The forces (F) are applied through pin support points (A, B, C, and D) within the adjustable distances (L_{AB}, L_{CD}).

Interface curvature (C): It was derived from the ratio of the projected area to the curved area, as expressed in Eq. (4). It was proposed as a parameter to describe the shape of the interface. Physically, it explained the percentage of the area that a connection can mobilize when resisting an external force.

$$C = \frac{A_{proj}}{A_{curved}} \times 100\%, \tag{4}$$

where C represents the interface curvature of a connection, which is the unitless area ratio; A_{proj} and A_{curved} denote the measured areas of the projected and curved surfaces, respectively, as explained in Fig. 3.

After the tensile test and the oven drying process, the fiber structure of the connection was examined by CT scanning (Phoenix Nanotom, 180 kV, 0.5 mA, with a resolution of 60 μm), as well as visual inspection after debarking. The examination focused on the merged fibers within the failure plane after the tests.

2.4. Tensile out-of-interface tests and mechanical properties

2.4.1. Tensile out-of-interface test setup

The tensile out-of-interface setup was designed with adjustable load-transfer clamps, as seen in Fig. 4. Two adjustable rails were fastened to the moving platform at the bottom and connected the load cell at the top, which provided a spatial four-point loading system, as illustrated in Fig. 4b and c. The analysis utilized 3D DIC cameras to gauge the interfacial region, with the ARAMIS (GOM, Germany) program used to assess deformations.

The schematic explanation of the load transfer pathway is presented in Fig. 4d. The tensile forces exerted by the supports (simplified as pins at points A, B, C, and D) were transferred to the interface of a connection. The distance L_{AB} and L_{CD} represented the load spans in two stems. These loading spans, excluding the interface width, were limited to twice the diameter size. The average ratio of span to diameter on each side of the stem was 0.88 with a CoV of 47%. This ensured that the forces conveyed to the interface were effectively treated as tensile forces acting on it. Controlled by a bottom loading platform, tensile testing was performed applying displacements. The platform moved at a constant velocity of 0.02 mm/s. During testing, the top clamp (located at A and B) remained immobile. The deformations of the connection were quantified by averaging the displacements at the loading points C and D. The measured deformations were at loading points C and D, and the local elongations were measured at the interface according to the shape of the connection, which will be explained in the result.

2.4.2. Determination of mechanical properties

The deformation curve of a connection could generally be divided into four regions: initial consolidation, elastic region, cracking region, and failure region, as shown in Fig. 5a. More detailed description will be presented in the Results section, according to different growth levels of connections. The maximum load (F_m) for a connection under tension was marked as point P in Fig. 5b. Points E and Q represented the 80% maximum loads during the ascending and descending stages of the deformation curve, respectively. Point M was where the force reaches $0.1F_m$, while point N corresponded to $0.4F_m$. The tangent drawn between the points M and N was used to calculate the elastic stiffness (K_e) of a connection. In addition, the initial stiffness (K_{e0}) was determined from the slope between the point M and the original O. Furthermore, from the peak point P to the original point O, the scant value of this region was determined as the peak stiffness (K_p). The expression for three stiffness can be found in Eq. (5).

$$K_e = \frac{0.4F_m - 0.1F_m}{S_4 - S_1}, \tag{5a}$$

$$K_{e0} = \frac{0.4F_m}{S_4}, \tag{5b}$$

$$K_p = \frac{F_m}{S_m}, \tag{5c}$$

where K_e, K_{e0}, and K_p represent the elastic stiffness, initial stiffness, and peak stiffness, respectively. F_m is the maximum force and its corresponding deformation is S_m. S_4 and S_1 are the deformation correspond to the force at 40% of F_m and 10% of F_m during the ascending process, respectively.

Tensile stresses were assumed to be evenly distributed in the projected area of the connection interface. Thus, the tensile strength of a connection, which was also considered as the effective strength, was the division of the maximum force by the projected area of the connection, expressed as Eq. (6).

$$f = \frac{F_m}{A_{proj}}, \tag{6}$$

where f denotes the strength of a connection, in MPa; F_m refers to the maximum force from the loading curve, and A_{proj} means the projected area of the connection.

2.5. Statistical analysis

Connections taken from different braided trees (see Table 1) may exhibit variations in properties (e.g., density and moisture content) due to differences in tree growth conditions (e.g., nutrition levels). To this end, a one-way ANOVA was performed to analyze parameters, such as density, moisture content, and cross-angle, to determine whether

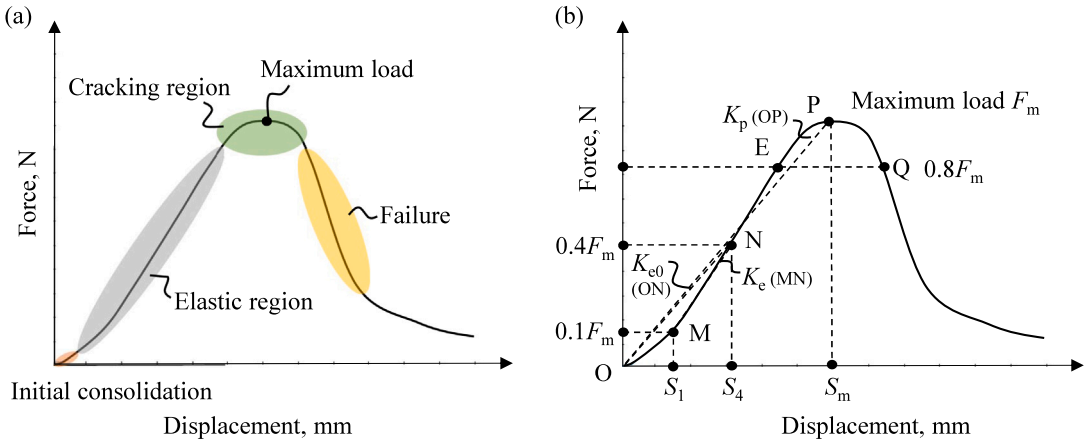

Fig. 5. Schematic illustration of the load–displacement behavior. (a) Representation of the load–displacement curve including regions of initial consolidation, elastic region, cracking region, and failure; (b) Details on the key points to determine mechanical properties (maximum load F_m, initial stiffness K_{e0}, elastic stiffness K_e, and peak stiffness K_p).

there were significant differences between braided tree structures. If the results were not significant, it would indicate that all connections could be reasonably analyzed further without considering the differences in their origin of growth. Furthermore, the obtained tensile strength of the connections was analyzed according to the spatial locations, with ANOVA distinguishing differences in lower, middle, and upper regions in the net of a braided tree structure. During this process, only green connections were included.

To describe the characteristics of the parameters measured from the connection, K–S tests were implemented. Nine parameters were examined, including the cone ratio, average diameter, diameter ratio, projected area, fusion degree, interface curvature, tensile strength, stiffness, and maximum load. This analysis was prepared to support further development of the prediction model for strength.

Before establishing the strength prediction model for the connections, the correlation between the measured parameters was analyzed and quantified using the coefficient of determination (r). A negative r indicates a negative relationship between two variables. When r is equal to 0, it means that there is no relation between the variables. An absolute value of r between 0.25 and 0.5 indicates a weak relationship. Between 0.5 and 0.75, a moderate relationship, and greater than 0.75 a strong correlation. Based on the results, different combinations of predictors were employed to compare and correlate with strength using multiple linear regression analysis.

3. Results and discussion

3.1. Description of the influencing parameters

Among the braided tree structures, the density showed weak significance and the cross-angle did not show significant differences, as indicated in Table 2. Thus, it can be assumed that there are no differences between braided tree structures. In contrast, the moisture content showed a noticeable difference. However, considering that the moisture content within the connections (more than 120%) is above the fiber saturation point, its influence on the material properties is assumed to be negligible. Therefore, it is considered reasonable to analyze connections from different trees for the comparison of mechanical properties. In addition, it can be assumed that the fibers of connections have similar material properties.

The results of the K–S tests are presented in Table 3. The results proved that all collected data were from normal distributions. The data of cone ratio showed slight variability (CoV 7.7%). However, the projected area (CoV 36.4%), fusion degree (56.9%), and maximum load (44.6%) showed considerable variability. Fusion degree and interface curvature are crucial indicators of the growth levels of the connections; and the high variability in the fusion degree (56.9%) indicates that the analysis covers a range of growth levels, which is important to understand how the tensile strength evolves as the connection matures.

Table 2
ANOVA results for parameters of braided tree structures.

Description	Null hypothesis: No difference among tree structures; Significance level: 5%.		
Parameters	F-value	p-value	Hypothesis
Density, kg/m^3	2.42	0.06	Accept
MC, %	38.58	2.30e−15	Reject
Cross-angle, degree	0.54	0.71	Accept

The distributions of diameter, interface curvature, fusion degree and tensile strength are plotted in Fig. 6. The morphology of the connections tested ranged from conditions where two stems were just connected in the bark to conditions where two centerlines of two stems were nearly in a plane. In the first case, the interface curvature can be considered to be close to 100% as the curved interface is nearly flat. In contrast, in the second case, when the two stems completely overlap, e.g., with a 90° cross angle, the interface curvature converges to around 30% when piths of stems overlap. Practically during the fusion process, if the tree stems fuse at a diameter of 2 mm and grow to a diameter of 20 mm, when a complete and sound fusion and co-growth is considered, the fusion degree converges to approximately 80%. This analysis attempts to point out that the ranges of growth parameters and mechanical properties are related to almost all growth levels. In other words, these ranges represent the development process of a connection in the course of its growth. In particular, the fusion degree studied ranged from −14.6% to 73.2%. Negative values in fusion degree were inevitable due to the stochastic and irregular growth pattern of trees; and it indicated that the connections did not merge well in the middle part and that the reaction wood may have caused an increase in volume, as discussed in [9,10].

In the measured connections, assuming that the analysis covered the full range of growth, it can be argued that the strength interval of a connection ranged approximately from the strength of the bark to the strength approximate to the wood fibers, from 0.23 to 1.38 MPa. The mean specific density of the connections studied was 0.332 g/cm^3 with a CoV of 12%. Limited research has been conducted on the strength of *Ficus* wood; therefore, reference is made to species with a specific density between 0.3 and 0.36 g/cm^3, such as spruce, fir, and cedar, which have tensile strengths perpendicular to the grain of 1.5, 1.2, and 1.9 MPa, respectively [18]. It can be estimated that the strength of

Table 3
Descriptive statistics and K-S tests results for parameters of self-growing connections.

Description	Null hypothesis: Tested data comes from a standard normal distribution; Significance level: 5%.				
Parameters	Mean	CoV (%)	[min, max]	*p*-value	Hypothesis
Cone ratio	0.91	7.7	[0.80, 1.00]	0.087	Accept
Average diameter, mm	20.1	15.9	[12.3, 26.8]	0.753	Accept
Diameter ratio	1.22	12.3	[1.00, 1.68]	0.15	Accept
Projected area, mm^2	964.8	36.4	[293.1, 2109.1]	0.253	Accept
Fusion degree, %	24.8	56.9	[-14.6, 73.2]	0.919	Accept
Interface curvature, %	56.9	18.5	[35.2, 89.8]	0.784	Accept
Tensile strength, MPa	0.75	29.3	[0.23, 1.38]	0.323	Accept
Elastic stiffness, N/mm	139.8	26.7	[55.3, 254.5]	0.992	Accept
Maximum load, N	718.3	44.6	[32.4, 1559.8]	0.332	Accept

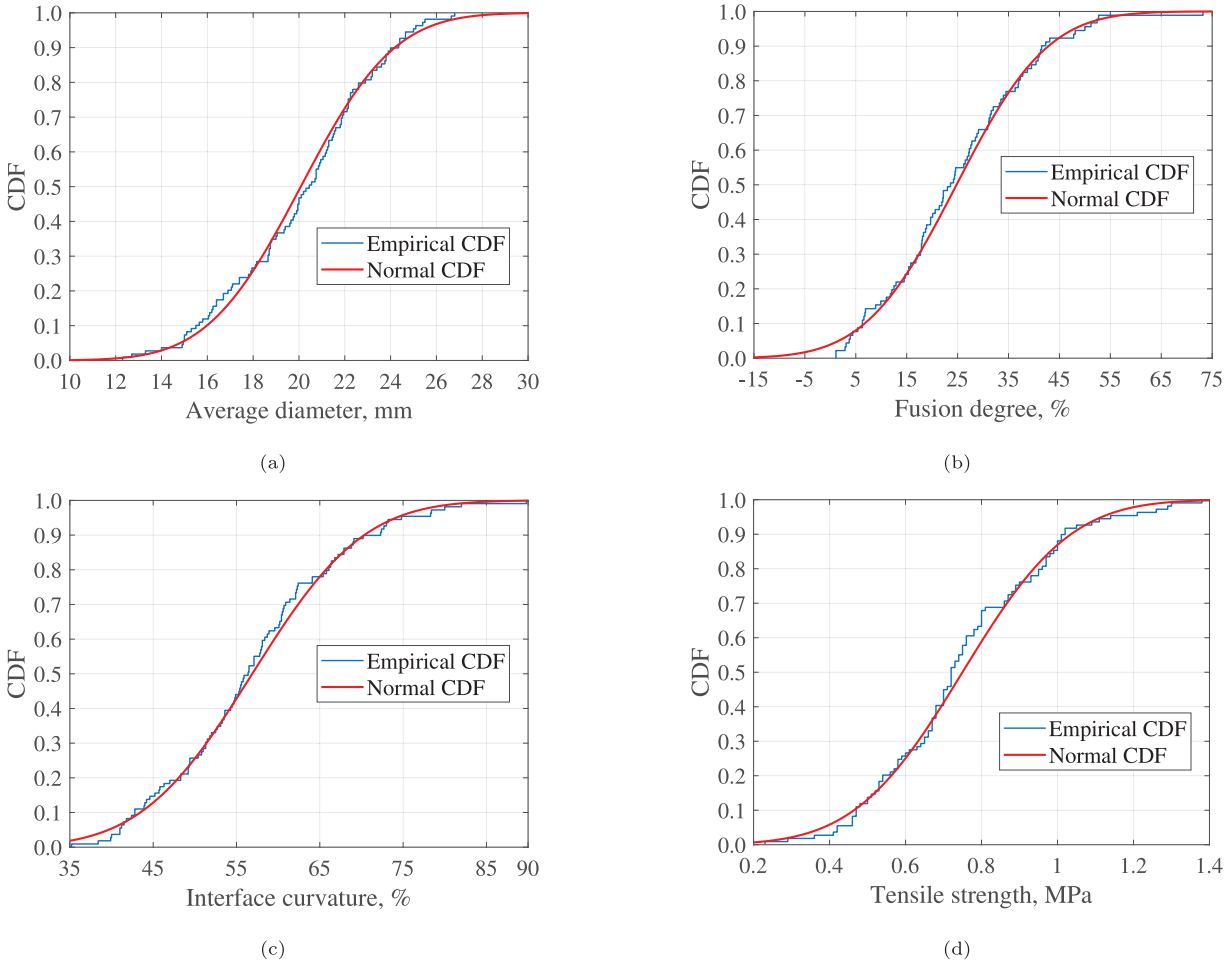

Fig. 6. Cumulative distribution functions (CDF) comparing measurements with normal distributions. (a) Average diameter; (b) Fusion degree; (c) Interface curvature; (d) Tensile strength.

the connection converges to the transverse tensile strength of the wood itself.

3.2. Tensile deformation behavior

Depending on the development pattern of the cracks within the connections, their mechanical performance can be categorized into two cases. The development of cracks in the first case follows the shape of the interface; and cracks in the second case deviate from the interface, which results in different behaviors and failure modes. The connection BB5 (Fig. 7a) and the connection BD11 (Fig. 8a) were used as representatives for the first and second cases, respectively. The connection BB5 has a diameter of 19.9 mm, a fusion degree of 13.2%, and an interface curvature of 61.7%. In contrast, the connection BD11 has a diameter of 19.7 mm, a fusion degree of 15.3%, an interface curvature of 53.6%. Three 20 mm long virtual strain gauges were installed at locations of lc1-middle, lc2-edge, and lc3-edge to measure local elongations. Lc1-middle was placed at the middle of the interface, and lc-edge and lc3-edge were placed 10 mm away from the middle gauge to inspect the developmental process of cracks.

After being subjected to tensile forces, connection BD11 initially experienced a short consolidation stage (Fig. 8b). During this period, the bark at the supporting location was compressed, and some water in the stems was compressed. Meanwhile, the connection adjusted its position because of its irregular shape until the equilibrium was

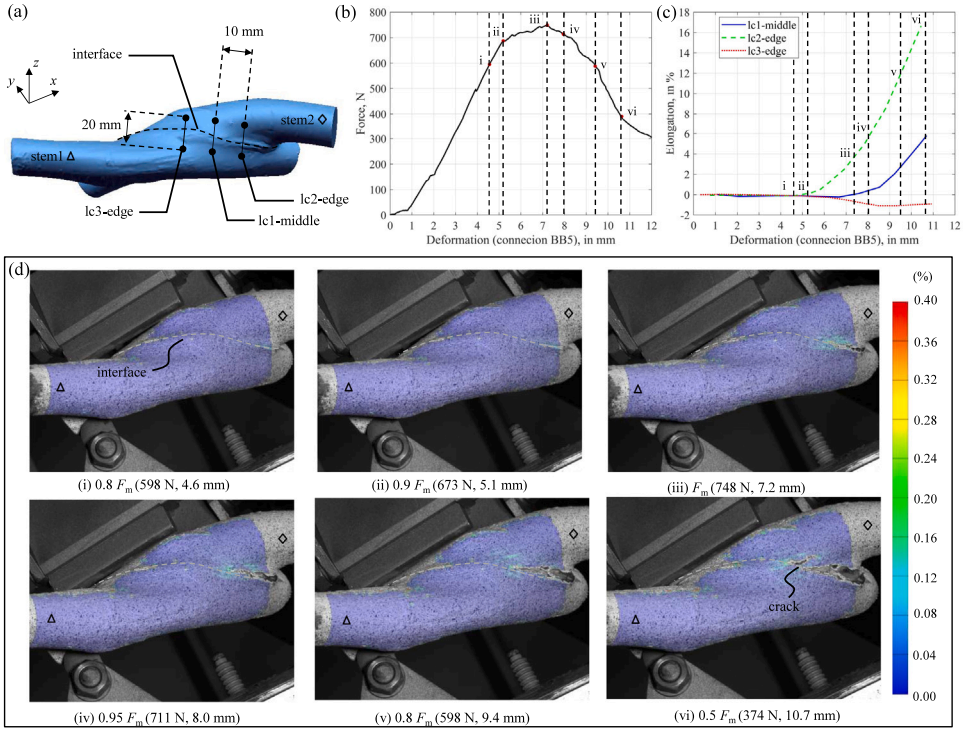

Fig. 7. Mechanical performance of connection BB5 and its failure at interface. (a) Schematic representation of the connection with locations of virtual strain gauges: lc1-middle, lc2-edge, and lc3-edge; (b) Force–deformation curve with different stages (i to vi) for connection BB5 under tension; (c) Elongation measured from strain gauges from (a); (d) DIC strain images at different stages of loading.

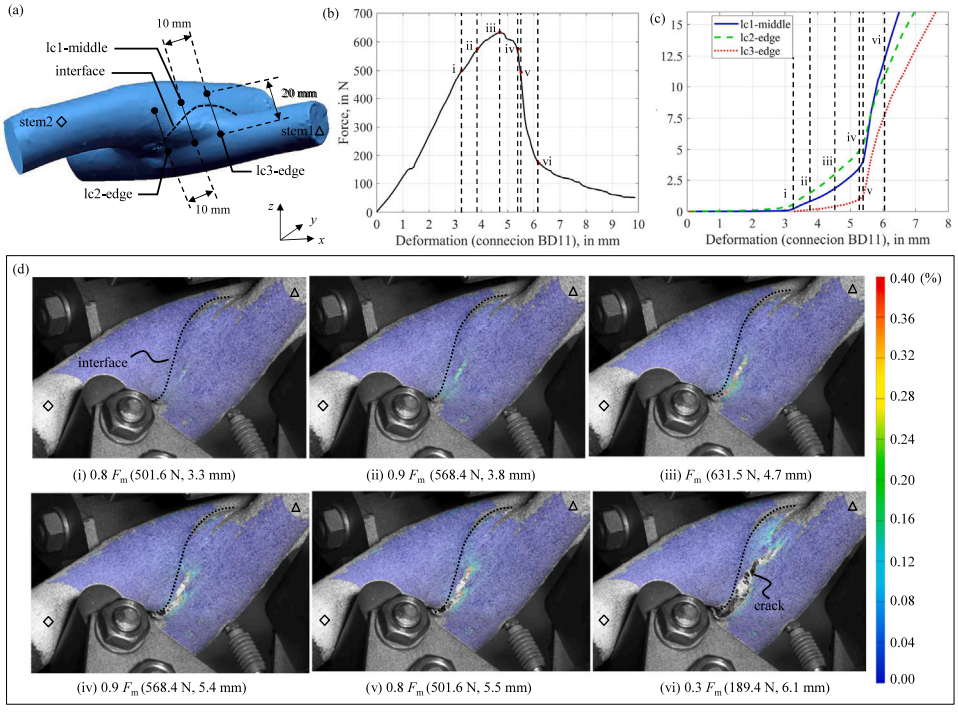

Fig. 8. Mechanical performance of connection BD11 and its failure across stems. (a) Schematic representation of the connection with locations of virtual strain gauges: lc1-middle, lc2-edge, and lc3-edge; (b) Force–deformation curve with different stages (i to vi) for connection BD11 under tension; (c) Elongation measured from strain gauges from (a); (d) DIC strain images at different stages of loading.

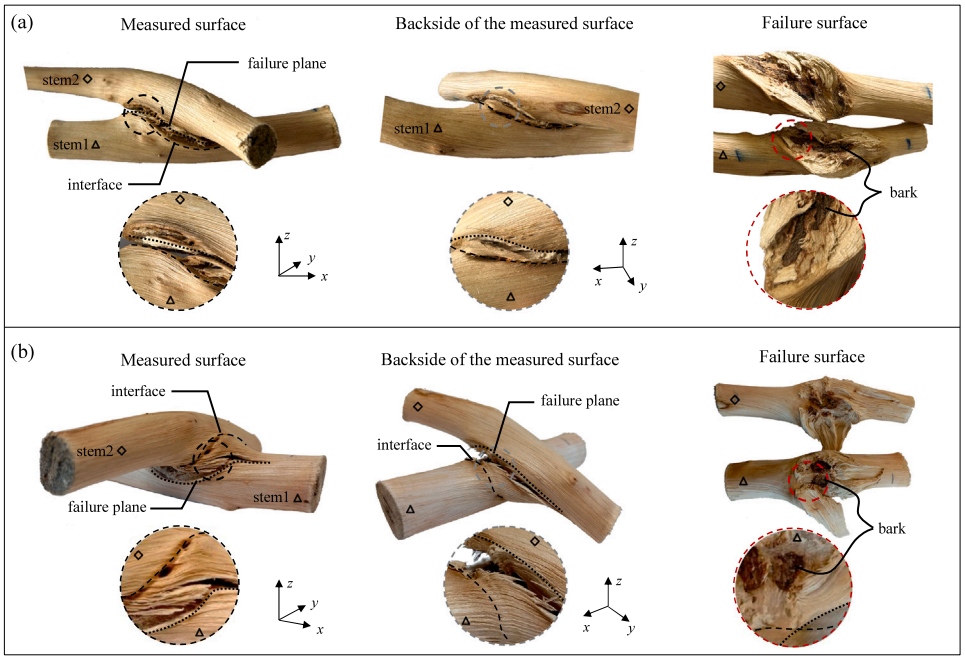

Fig. 9. Failure modes of self-growing connections. (a) Failure mode I: Failure at the interface; (b) Failure mode II: Failure across stems. (For interpretation of the references to color in this figure legend, the reader is referred to the web version of this article.)

reached. In comparison, the consolidation stage of connection BB5 was longer with a displacement of 1 mm (Fig. 7b).

Following the consolidation stage, the connection underwent a linear elastic phase characterized by a proportional increase in forces with displacement. The deformation in this stage resulted from two parts: initial deformation on the four sides of the stems and subsequent elongation in the intersected region. Although the distance between the loading point and the edge of the interface was controlled to be less than 4 cm, bending moments transferred from the support to the interface was inevitable.

After the linear region, the extension of the cracks differentiated the failure mechanisms. In the ascending stage after linear deformation, the stiffness of the connections was reduced and resulted in the nonlinearity in the cracking region in the deformation curve (stage i to iii in Figs. 7b and 8b). Cracks were first observed at the edge of the interface (stage i at the edge location in Figs. 7d, and 8d). In this location, the material mainly consisted of bark tissues with minimal fused fibers, as shown in Fig. 1c. At this point, the force typically reached approximately 0.8 F_m (Figs. 7b and 8b). With increasing forces, the crack spread to the interface, as evidenced by the increase in elongation in the middle of the interface (in the middle location in Figs. 7c and 8c). During the cracking process, the measurements in lc1-middle rose (tensioned) when the measured surface cracked (lc1-middle in Fig. 7c), while this location could be compressed (lc1-middle in Fig. 8c) when cracking occurred on the backside of the monitoring surface. The wood material is usually considered brittle [19,20]. Thus, the propagation of the crack in both x and y directions, combined with the rotation of the stem, caused nonlinearity in the deformation curve. It was observed that when the crack extended to approximately half of the interface area, around 0.8 F_m in the descending stage of the curve (stage v in Figs. 7d and 8d), the connection experienced a sudden load drop followed by subsequent failure.

3.3. Failure modes of connections

The above two connections are representative of the two types of mechanical responses observed. The difference in their failure was mainly attributed to their growth levels. In other words, the failure was mainly influenced by the morphology of the merged fibers. Therefore, two failure modes were distinguished: failure at the interface (FM I, Fig. 9a) and failure across stems (FM II, Fig. 9b). To be specific, the failed surface in FM I occurred mainly at the interface of a connection. However, in FM II, the failed surface consisted of a part of the interface and a partial area in the stems, which is called failure across stems. The cracking fibers in different cross sections can be seen in Fig. 10 for FM I and Fig. 11 for FM II.

In failure mode I (Figs. 9a and 10), the cracking surface (black dashed line) overlapped the interface (red dashed line) in each cross section (Fig. 10b to g, red circles). Although a small number of merged fibers were found within the connection in Figs. 9a, 10b and c, they failed to form an effective bond between the two stems. The resulting tensile strength of the connection was 0.5 MPa.

In contrast, in failure mode II (Figs. 9b and 11), the failure surface (black dashed line) only partially overlapped the interface (red dashed line). Connections that failed in FM II had more merged fibers and formed a more curved interface. As seen in the failure pattern of failure mode II (Fig. 8), cracks occurred first at the corners and then extended along the interface (Fig. 11b to c). However, when the crack extension encountered the merged fibers (Fig. 11c to e), the crack path no longer followed the interface, but instead followed the direction of the wood grain (also see Fig. 9b). The connection BD11 presented a tensile strength of 0.75 MPa, which was higher than the connection BB5. To compare the failure plane with the interface and the merged fiber direction in Figs. 9b and 11, it was argued that the failure occurred mainly due to a combination of the tensile strength limit of soft tissues, the shear strength limit, as well as the tensile strength limit perpendicular to the wood grain.

When the two failure modes are differentiated according to the fusion degree and interface curvature, the results are shown in Fig. 12. Both failure modes tended to be normally distributed for these parameters. Regarding the fusion degree, from Fig. 12a, the second failure mode was more likely to occur than the first, when the fusion degree was greater than approximately 15%. However, it was not significant to use the interface curvature to distinguish failure modes (Fig. 12b). This

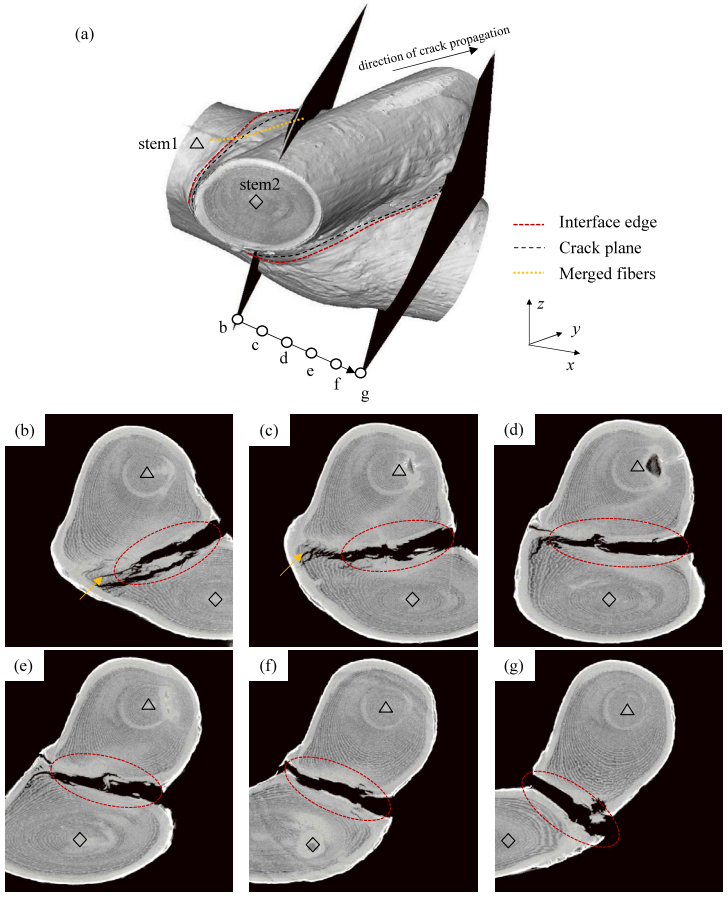

Fig. 10. Fiber cracking at different cross sections in failure modes I of connection BB5. (a) CT scanning of connection BB5 and the cross sections taken for visualization; Cross sections (b) to (g) from the scanning results of connection BB5 in (a). (For interpretation of the references to color in this figure legend, the reader is referred to the web version of this article.)

may be due to the more pronounced adaptive growth of connections in the radial direction. Moreover, fusion degree presents a wider range than the interface curvature.

3.4. Comparison of mechanical properties under various conditions

3.4.1. Comparison of strength and loading capacity in two failure modes

When comparing the strengths in the two failure modes, the strength in failure mode II was slightly stronger than that of failure mode I ($p = 0.0018 < 0.05$, significant) (Fig. 13a). Furthermore, connections that failed in the second mode had a higher loading capacity ($p = 00082 < 0.05$, significant) (Fig. 13b). This means that as the degree of growth increases, the strength and load carrying capacity of the connection may also increase. This can be explained by more merged fibers growing in the interconnected region which reinforce the resistance of a connection.

3.4.2. Comparison of stiffness at different stages under tension

The stiffness defined according to Eq. (5) is compared in Fig. 14. A comparison of stiffness including the initial phase and the linear phase showed that most connections had an initial consolidation phase (Fig. 14a). This observation suggested that the stiffness of a connection would be more accurate in terms of the linear stage after the initial phase was removed. In initial consolidation, adjustments of the connection moisture and shape can affect the initial loading. The stiffness during the elastic stage was higher compared to the calculation of the peak stage (Fig. 14b). This indicated the period where the connections present the nonlinearity during the performance. Therefore, in order to better describe the stiffness of a connection, it is more appropriate to take the linear phase into consideration.

3.4.3. Comparison of strength at different moisture levels and tree sizes

The tensile strength analyzed under different conditions is compared in Fig. 15. The tensile strength of the connections in different spatial locations was analyzed by ANOVA (Fig. 15a), which showed that there was no significant difference ($p = 0.1485 > 0.05$) in the tensile strength at the three spatial locations (lower, middle, and upper). This argues that the effect of spatial locations on the tensile strength of connections can be neglected.

In contrast, the effect of moisture content and diameter size on the strength of connections cannot be ignored. The strength of dry connections was higher than that of all wet connections (Fig. 15b). This is because dry wood material is considered stronger than wet wood [18,21]. In general, connections with smaller diameters provided less strength than larger connections. This may be related to the strength of wood at different ages and density, because larger diameters indicate more mature wood and higher density compared to smaller diameters [22,23]. This analysis illustrates the dynamic changes in the strength of the connections during their growth process. It also demonstrates that connections can still present significant mechanical strength and value even after their death.

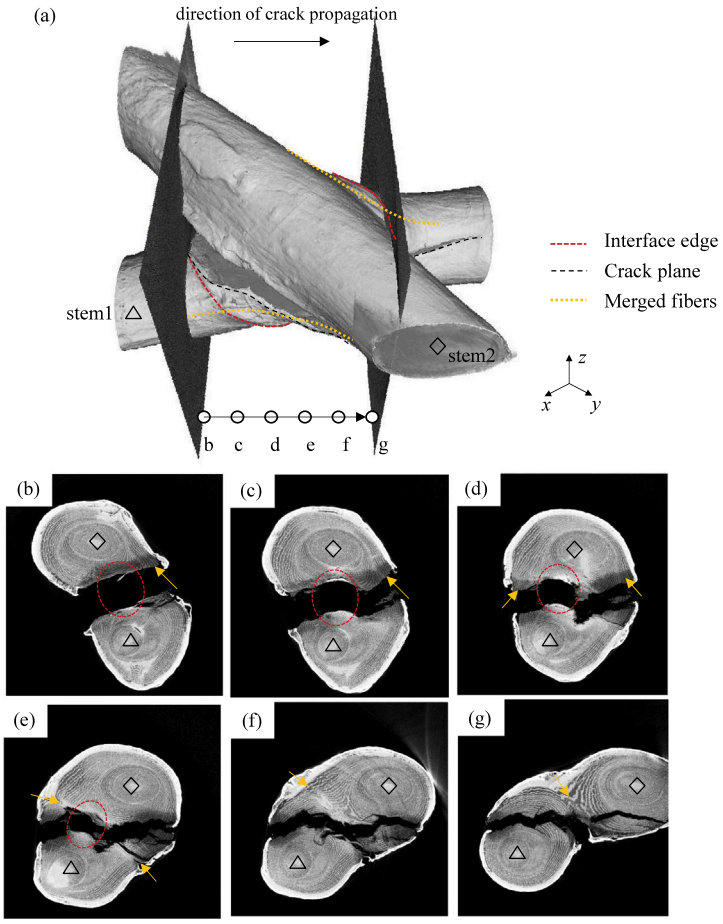

Fig. 11. Fiber cracking at different cross sections in failure modes II of connection BD11. (a) CT scanning of connection BD11 and the cross sections taken for visualization; Cross sections (b) to (g) from the scanning results of connection BD11 in (a).

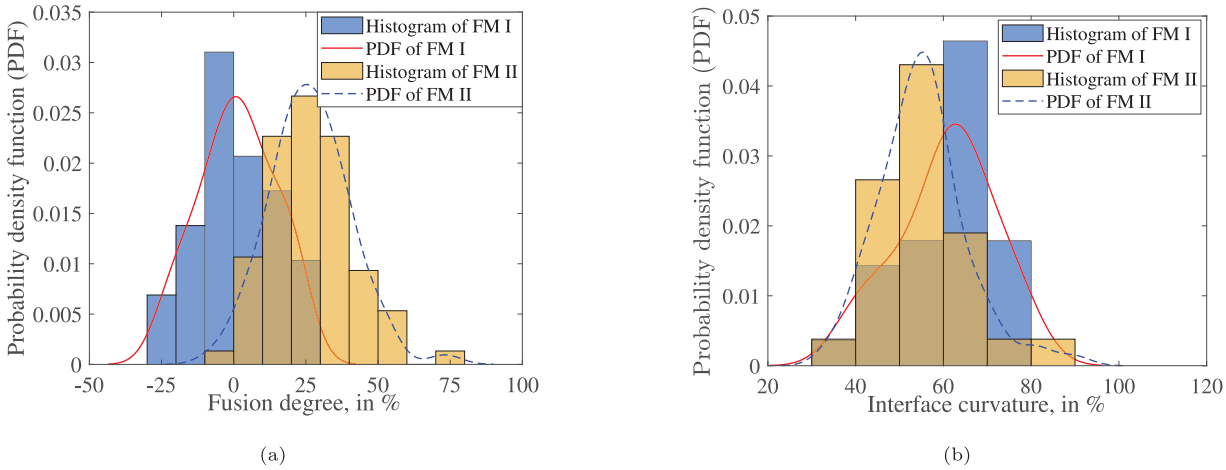

Fig. 12. Two failure modes (FM I and FM II) differentiated by fusion degree (a) and interface curvature (b).

3.5. Evaluation of mechanical properties and tensile strength prediction for connections

3.5.1. Correlation between influencing parameters and mechanical properties

Fig. 16 gives an overview of the distribution of the measured influencing parameters and mechanical properties, as well as the correlation between them. From the correlation between the influencing parameters and the mechanical properties, the diameter of the stem had good correlations with the projected area of the interface (r = 0.72), stiffness (r = 0.70), and maximum loading capacity (r = 0.84). However, the fusion degree only weakly correlated with diameters. The cone ratio and diameter ratio did not significantly influence the mechanical properties of the connections. The projected area of the connection was strongly correlated with the stiffness (r = 0.66) and the maximum load (r = 0.74) of the connection. Of the two parameters

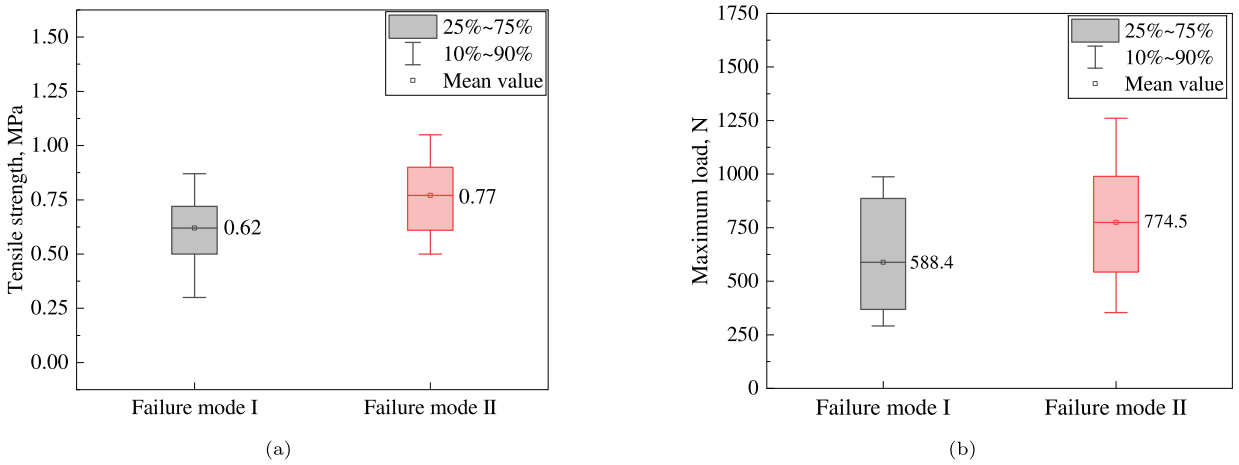

Fig. 13. Comparisons of strength and maximum load of two failure modes. (a) A comparison of tensile strength; (b) A comparison of maximum load.

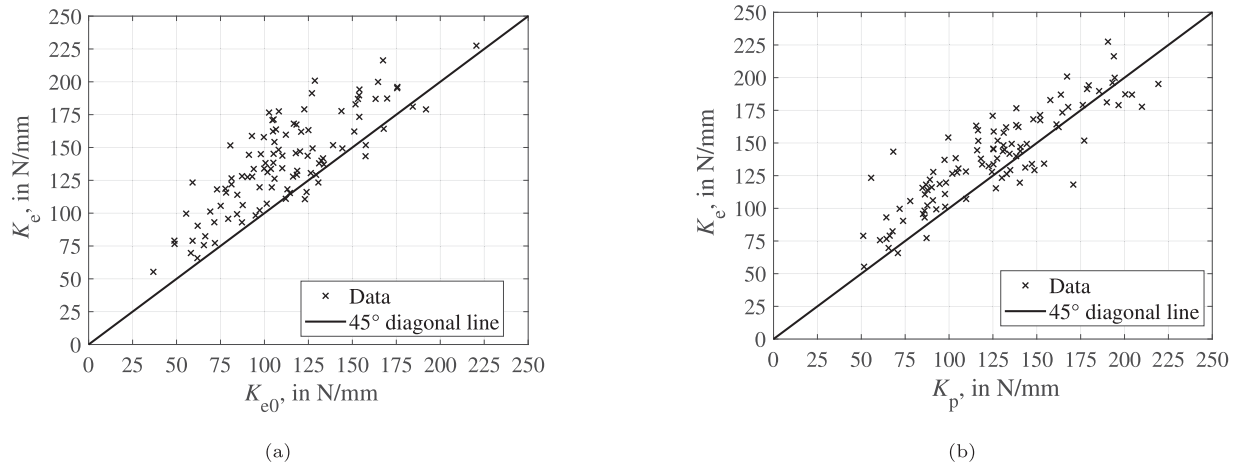

Fig. 14. Comparisons between calculations of stiffness, according to Eq. (5). (a) A comparison between elastic stiffness (K_e) and initial stiffness (K_{e0}); (b) A comparison between elastic stiffness and peak stiffness (K_p).

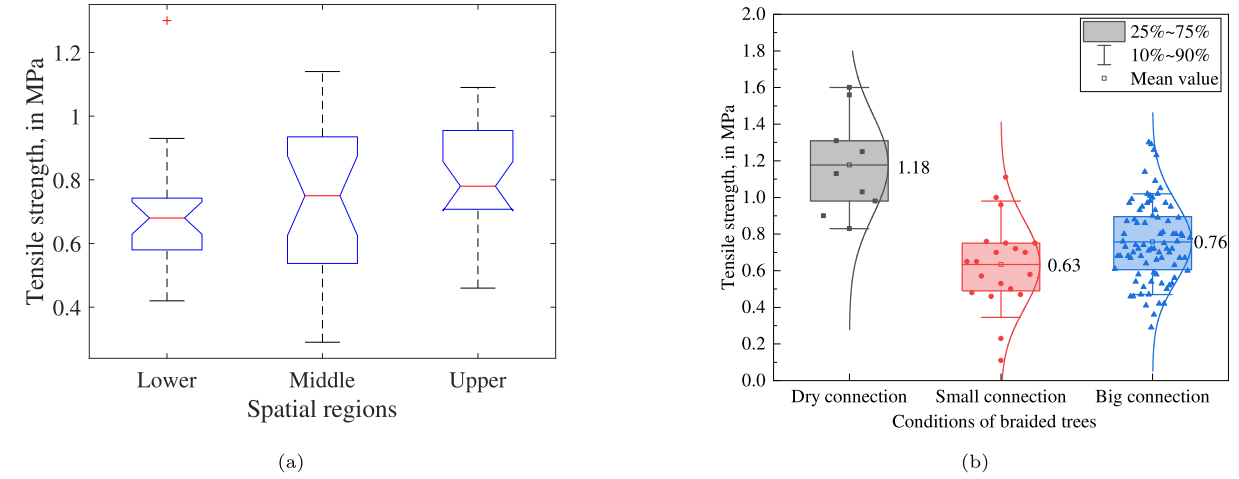

Fig. 15. Comparisons among connections in different conditions. (a) A strength comparison among connections in three spatial locations (lower, middle, and upper) in braided trees, and the top and bottom edges of the box indicate 25 to 75th percentile; (b) A strength comparison between connections in three types of braided trees (dry, small and big as in Table 1).

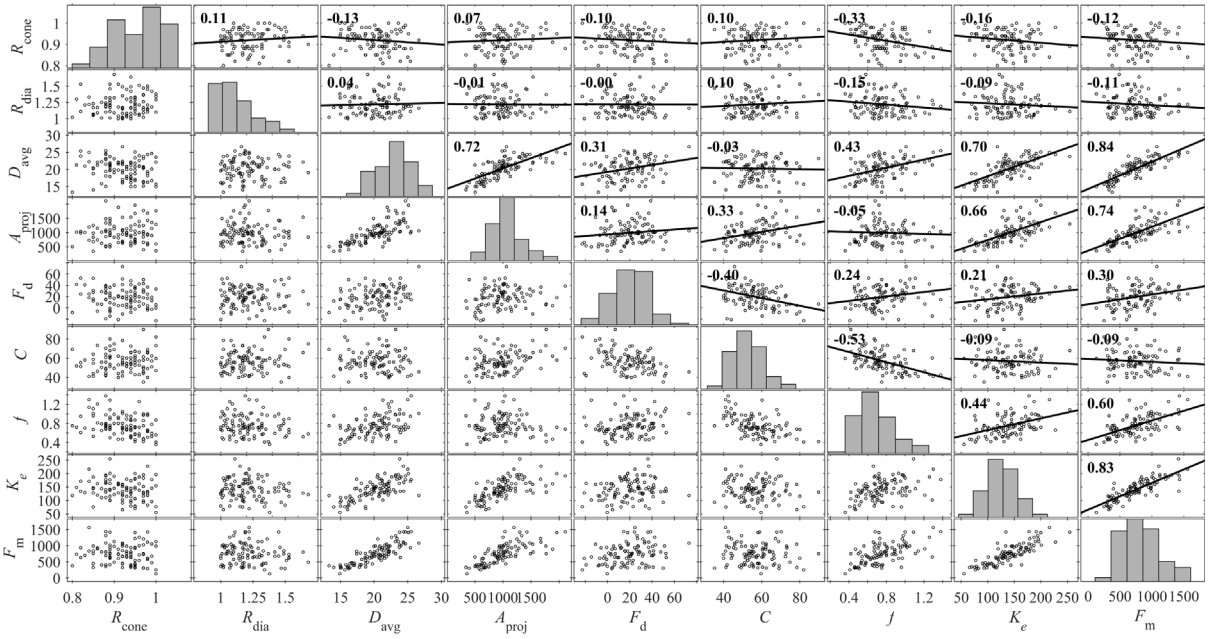

Fig. 16. Correlation matrix among parameters: Cone ratio (R_{cone}), diameter ratio (R_{dia}), diameter (D_{avg}), projected area (A_{proj}), fusion degree (F_d), interface curvature (C), strength (f), elastic stiffness (K_e), and maximum load (F_m).

proposed to describe the growth level, the interface curvature ($r = -0.53$) was a better predictor of connection strength than the fusion degree ($r = 0.24$). Notably, interface curvature correlated negatively with the tensile strength. It indicates that a flatter interfacial area results in lower connection strength. Among the parameters, diameters and interface curvature are good predictors of the mechanical properties of connections.

3.5.2. Prediction of tensile strength of a connection

Based on the results of correlation analysis on the strength of a connection, the measured parameters included diameter ratio, cone ratio, average diameter, projected area, fusion degree, and interface curvature. Multiple linear regressions were performed using different combinations of influencing parameters. The groups of different combinations can be seen below.

$$f = -0.68R_{cone} + 0.00014A_{proj} - 0.0017F_d - 0.013C + 2.0 \quad R^2 = 0.31 \tag{7a}$$

$$f = -0.70R_{cone} + 0.032D_{avg} - 0.0027F_d - 0.012C + 1.4 \quad R^2 = 0.47 \tag{7b}$$

$$f = -0.69R_{cone} + 0.00012A_{proj} + 0.0014F_d + 1.8 \quad R^2 = 0.06 \tag{7c}$$

$$f = -0.58R_{cone} + 0.00012A_{proj} - 0.012C + 1.8 \quad R^2 = 0.30 \tag{7d}$$

$$f = -0.44R_{cone} - 0.24R_{dia} + 0.050D_{avg} - 0.00022A_{proj} - 0.0020F_d - 0.0082C + 1.2 \quad R^2 = 0.54 \tag{7e}$$

The results of each combination are given in Fig. 17. Compared with groups Eqs. (7a) and (7b), although the diameter correlated with the projected area, the prediction of using diameter was more significant. Similarly, the fusion degree weakly correlated with the interface curvature; and the interface curvature predicted the results better than fusion degree (groups Eqs. (7c) and (7d)). However, the prediction accuracy was only 54% when all the measured parameters were considered.

Several factors contribute to this limited accuracy. The inhomogeneous properties of wood and the stochastic growth of trees introduce variability in the characteristics of the material [24,25]. For example, different parts of the wood have different strengths [26]. Mature wood is considered stronger than juvenile wood [27]; and wood with different cambial ages has varies properties [28]. Tension wood has a higher tensile strength than regular wood because tension wood has more cellulose [29]. The existing measured parameters may not fully quantify all growth characteristics, such as the angle and volume of the merged fibers. In addition, other growth characteristics, such as the higher density on the intersected surface, need to be reasonably quantified to improve the accuracy of the prediction.

3.5.3. Further insights into tensile failure mechanisms

To measure the strength of a connection, this study used an approximate approach. It assumed that the loading forces were uniformly transmitted to the effective interface perpendicular to the loading direction. However, the stress environment at the interface is complex and involves the interaction of shear and tensile stresses. The fiber orientation varies significantly at different positions along the interface [9,10], as shown at points P_1, P_2, and P_3 in Fig. 18. When applying a tensile force F, the corner at P_1, which lacks continuous fibers, relies mainly on the bark tissue to bear the tensile stress (Fig. 18b and c). In contrast, at point P_2, the tensile stress can be understood as a resultant of perpendicular tensile and shear stresses (Fig. 18d and e) along the direction of local fibers. The materials in P_3 experience a similar stress environment, but the orientation of the fiber differs from P_2 (Fig. 18d and f). Therefore, the failure strength of the interface is a combination of the limits of the tensile perpendicular (stress $\sigma_{t,90}$, strength $f_{t,90}$) and shear strength (stress σ_v, strength f_v). The failure criteria can be expressed in Eq. (8).

$$\left(\frac{\sigma_{t,90}}{f_{t,90}}\right)^2 + \left(\frac{\sigma_v}{f_v}\right)^2 \le 1 \tag{8}$$

As the self-growing connection grows, the improvement in connection's quality is primarily reflected in the increase in the amount of merged fibers and their optimized orientations. However, quantifying merged fibers through non-destructive methods is challenging. Therefore, based on understanding the relationship between the growing dimensions and the internal structure [9,10], this study used the fusion degree and interface curvature as indirect and non-destructive indicators of the quality of the connection. Estimating tensile strength of a connection based on the strength of base materials (i.e., strength of

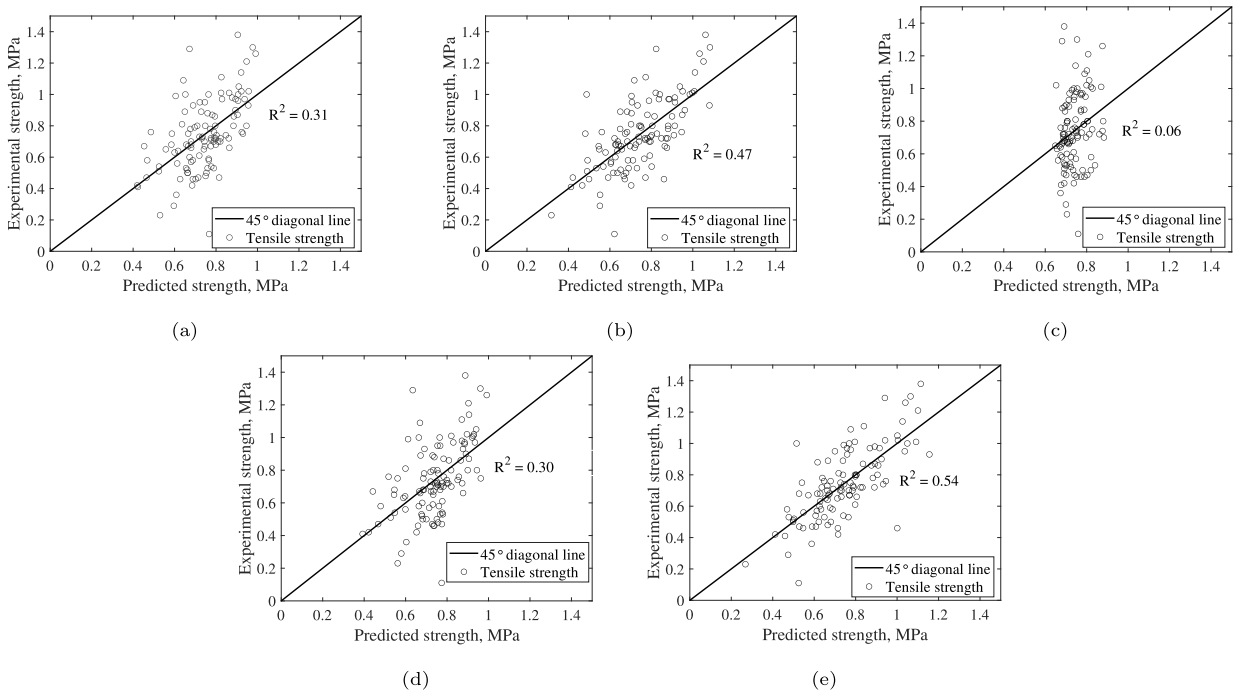

Fig. 17. Results of multiple linear regression. (a) Results of Eq. (7a); (b) results of Eq. (7b); (c) results of Eq. (7c); (d) results of Eq. (7d); (e) results of Eq. (7e).

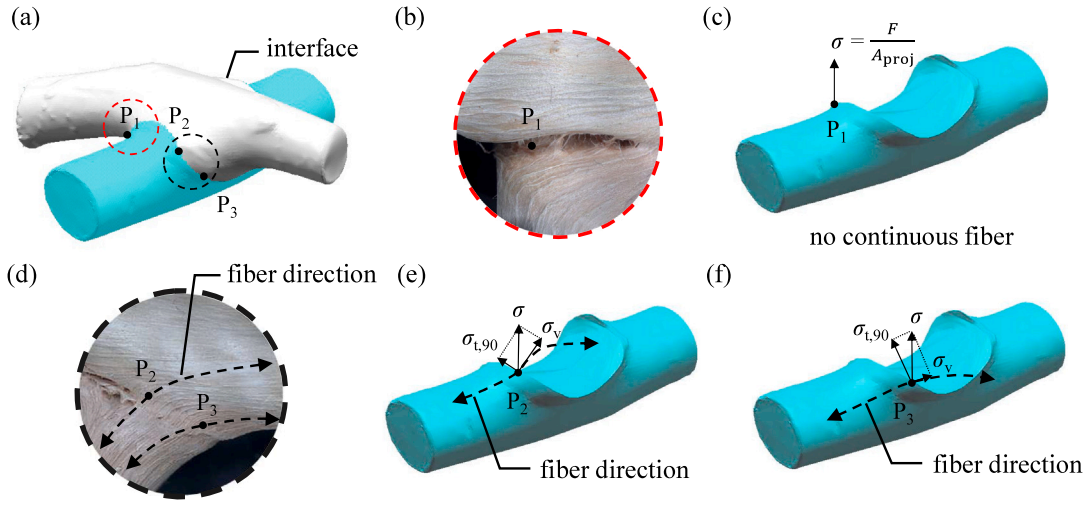

Fig. 18. Illustration of the stress and fiber orientation at different points along the interface. (a) Overview of points P_1, P_2, and P_3 at the interface; (b) Fiber morphology of the area in a red circle in (a); (c) At point P_1, no continuous fiber resists tensile stress (σ). (d) Fiber orientations at points P_2 and P_3; area in the black circle is zoomed in (a). (e) Stress components at P_2, indicating the interaction of perpendicular tensile stress ($\sigma_{t,90}$), and shear stress (σ_v). (f) Stress components at P_3 according to the direction of the local fiber.

fibers from material tests) is physically more direct. However, it still requires understanding how growth variations affect the morphology of merged fibers during growth. Furthermore, when conducting material tests on base fibers, high moisture content and small specimen size (diameter less than 30 mm) present challenges to the fabrication of samples and therefore affect the accuracy of measurements. For instance, high moisture content can easily cause slippage, which may compromise the reliability of measurements.

4. Conclusion

In this paper, the mechanical properties and developmental growth levels of self-growing connections formed by *Ficus* were studied. Developmental growth levels were quantified by fusion degree and interface curvature. Mechanical properties were investigated by designing a loading set-up that was adaptable to the irregular geometry of the connections. The following conclusions are drawn.

1. Regarding *Ficus* connections, with developmental growth levels ranging from initial formation to approximate piths fusion, the tensile strength ranges from 0.23 to 1.38 MPa.
2. The patterns of crack development in connections are related to the morphology of merged fibers. The inhomogeneous distribution of merged fibers, the two-dimensional extension of cracks, together with the irregular shape of connections, result in a nonlinear stage in the cracking region.
3. The failure modes of connections can be categorized into two: Failure at the interface (FM I) and failure across stems (FM

II). Connections under FM II present greater strength and load-bearing capacity than those under FM I. It is more effective to distinguish two failure modes by fusion degree of a connection. A connection tends to fail in FM II when its fusion degree is greater than approximately 15%.

4. Regarding the *Ficus* braided trees, different spatial locations do not lead to significant effects, and dry connections are significantly stronger than wet connections.
5. Statistical analysis shows that diameter size has the most significant effect on mechanical properties. Interface curvature shows a moderately negative correlation with strength. Interface curvature, fusion degree, and diameter size can be effective predictors of strength.

Future work may analyze the connections formed by different tree species to compare with the *Ficus* connections. In addition to tensile tests, shear tests for connections can be designed to analyze the ultimate load-carrying capacity under different loading conditions. The quantitative parameters for developmental growth may not be sufficient in this work. Future work may develop a method that can accurately describe the merged fibers to improve the accuracy of the prediction.

The analysis in this paper can predict and analyze dry and green connections, while it can also predict the strength of a connection grow dynamically. This offers a strong reference for nature-based design.

CRediT authorship contribution statement

Xiuli Wang: Writing – original draft, Visualization, Methodology, Investigation, Formal analysis, Data curation, Conceptualization. **Wolfgang Gard:** Writing – review & editing, Supervision, Conceptualization. **Jan-Willem van de Kuilen:** Writing – review & editing, Supervision, Project administration, Funding acquisition.

Declaration of competing interest

The authors declare that they have no known competing financial interests or personal relationships that could have appeared to influence the work reported in this paper.

Acknowledgments

The authors acknowledge the funding from China Scholarship Council (CSC) and the partial funding support from Deutsche Forschungsgemeinschaft (DFG), entitled Natürlich gewachsene Holzelemente als Basis für tragende Konstruktionen – Statische Analyse und Wachstumssimulation. (Project number: 512769030). The support of Giorgos Stamoulis during the tests is also greatly appreciated.

Data availability

Data will be made available on request.

References

[1] F.W. Telewski, M.J. Jaffe, Thigmomorphogenesis: Anatomical, morphological and mechanical analysis of genetically different sibs of *Pinus taeda* in response to mechanical perturbation, Physiol. Plant. 66 (2) (1986) 219–226.
[2] O. Hamant, M.G. Heisler, H. Jonsson, P. Krupinski, M. Uyttewaal, P. Bokov, F. Corson, P. Sahlin, A. Boudaoud, E.M. Meyerowitz, et al., Developmental patterning by mechanical signals in *Arabidopsis*, Science 322 (5908) (2008) 1650–1655.
[3] B. Moulia, S. Douady, O. Hamant, Fluctuations shape plants through proprioception, Science 372 (6540) (2021) eabc6868.
[4] E. Badel, F.W. Ewers, H. Cochard, F.W. Telewski, Acclimation of mechanical and hydraulic functions in trees: Impact of the thigmomorphogenetic process, Front. Plant Sci. 6 (2015) 266.
[5] T. Alméras, M. Fournier, Biomechanical design and long-term stability of trees: Morphological and wood traits involved in the balance between weight increase and the gravitropic reaction, J. Theoret. Biol. 256 (3) (2009) 370–381.
[6] X. Wang, W. Gard, H. Borska, B. Ursem, J.W.G. van de Kuilen, Vertical greenery systems: From plants to trees with self-growing interconnections, Eur. J. Wood Wood Prod. 78 (2020) 1031–1043.
[7] F. Ludwig, H. Schwertfreger, O. Storz, Living systems: Designing growth in baubotanik, Archit. Des. 82 (2) (2012) 82–87.
[8] F. Ludwig, W. Middleton, F. Gallenmüller, P. Rogers, T. Speck, Living bridges using aerial roots of *Ficus elastica*–an interdisciplinary perspective, Sci. Rep. 9 (1) (2019) 12226.
[9] X. Wang, Build with nature: Biomechanical properties and performance of self-growing connections in interconnected trees (Ph.D. thesis), Technology University of Delft, 2024.
[10] X. Wang, W. Gard, Y. Mosleh, J.W.G. van de Kuilen, Morphological analysis of inosculated connections in weeping figs: Insights on density, geometry, fiber structures, and compositional variations, Wood Sci. Technol. 59 (24) (2025).
[11] C. Mattheck, Wood-the internal optimization of trees, Arboricult. J. 19 (2) (1995) 97–110.
[12] T. Lievestro, Living trees as structural elements for vertical forest engineering, Delft University of Technology, 2020.
[13] B. Kane, R. Farrell, S.M. Zedaker, J.R. Loferski, D.W. Smith, Failure mode and prediction of the strength of branch attachments, Arboric. Urban For. 34 (5) (2008) 308–316.
[14] D. Slater, A.R. Ennos, Determining the mechanical properties of hazel forks by testing their component parts, Trees 27 (2013) 1515–1524.
[15] G.A. Dahle, Influence of bark on the mapping of mechanical strain using digital image correlation, Wood Sci. Technol. 51 (6) (2017) 1469–1477.
[16] J. Tippner, L. Praus, M. Brabec, V. Sebera, B. Vojáčková, J. Milch, Using 3D digital image correlation in an identification of defects of trees subjected to bending, Urban For. Urban Green. 46 (2019) 126513.
[17] E.U. for Standization, EN13183-1: Moisture content of a piece of sawn timber - Part 1: Determination by oven dry method, 2002.
[18] D. Kretschmann, Mechanical properties of wood, in: Wood Handbook: Wood as an engineering material: Chapter 5, Vol. 190, 2010, pp. 1–46.
[19] C. Sandhaas, J.W.G. van de Kuilen, Strength and stiffness of timber joints with very high strength steel dowels, Eng. Struct. 131 (2017) 394–404.
[20] C. Sandhaas, A.K. Sarnaghi, J.W.G. van de Kuilen, Numerical modelling of timber and timber joints: Computational aspects, Wood Sci. Technol. 54 (2020) 31–61.
[21] R.R.N. Mvondo, P. Meukam, J. Jeong, D.D.S. Meneses, E.G. Nkeng, Influence of water content on the mechanical and chemical properties of tropical wood species, Results Phys. 7 (2017) 2096–2103.
[22] H.C. Spatz, J. Pfisterer, Mechanical properties of green wood and their relevance for tree risk assessment, Arboricult. Urban For. 39 (5) (2013) 218–225.
[23] B. Guller, K. Isik, S. Cetinay, Variations in the radial growth and wood density components in relation to cambial age in 30-year-old *Pinus brutia* Ten. at two test sites, Trees 26 (2012) 975–986.
[24] T. Speck, I. Burgert, Plant stems: Functional design and mechanics, Annu. Rev. Mater. Res. 41 (1) (2011) 169–193.
[25] M. Fournier, V. Decoux, A. Stokes, K. Faiers, F. Salin, D. Guitard, Integrative biomechanics for tree ecology: Beyond wood density and strength, J. Exp. Bot. 64 (15) (2013) 4793–4815.
[26] P.K. Dadzie, M. Amoah, Density, some anatomical properties and natural durability of stem and branch wood of two tropical hardwood species for ground applications, Eur. J. Wood Wood Prod. 73 (2015) 759–773.
[27] F. Bao, Z. Jiang, X. Jiang, X. Lu, Differences in wood properties between juvenile wood and mature wood in 10 species grown in China, Wood Sci. Technol. 35 (2001) 363–375.
[28] M. Ivković, H.X. Wu, C. Matheson, D. South, T.A. McRae, C.A. Raymond, Influence of cambial age and climate on ring width and wood density in *Pinus* radiata families, Ann. Forest Sci. 70 (2013) 525–534.
[29] B. Clair, T. Alméras, H. Yamamoto, T. Okuyama, J. Sugiyama, Mechanical behavior of cellulose microfibrils in tension wood, in relation with maturation stress generation, Biophys. J. 91 (3) (2006) 1128–1135.